J. Earth Syst. Sci. (2020)129 47
https://doi.org/10.1007/s12040-019-1308-1

Petrological study of spinel peridotites of Nidar ophiolite, Ladakh Himalaya, India

Ranjit Nayak[1,2,*] and Bidyananda Maibam[3]

[1]*Department of Earth and Atmospheric Sciences, NIT Rourkela, Rourkela 769 008, India.*
[2]*Department of Geology, Addis Ababa Science and Technology University, Addis Ababa, Ethiopia.*
[3]*Department of Earth Sciences, Manipur University, Canchipur, Imphal 795 003, India.*
**Corresponding author. e-mail: nayak.ranjit213@gmail.com*

MS received 12 March 2019; revised 24 September 2019; accepted 9 October 2019

Petrological study of the ultramafic rocks from the Nidar Ophiolite Complex (NOC) of the Indus Suture Zone is carried out. The study of Cr-spinels along with olivine and pyroxenes emphasizes the genesis and tectonic setting of the ultramafites. Olivine from the harzburgite is Mg-rich, with the molar ratio Mg# [Mg/(Mg + Fe^{2+})] varying between 0.91 and 0.94 and olivine in dunite between 0.92 and 0.94. Clinopyroxene from the harzburgite is TiO_2 and Na_2O-poor diopside ($Wo_{47–50}En_{47–50}Fs_{2–4}$). Spinel in harzburgite shows wide Cr#, molar ratio varied between 0.26 and 0.72, and significantly higher in dunites with Cr# ranges from 0.69–0.85. Cr# of the peridotite spinel follow a depletion trend. Calculated equilibrium conditions of the samples are 800–900°C temperature, 32 and 40 kbar pressure, oxygen fugacity −0.09 to 0.55 log units above the FMQ buffer. Residual nature of the harzburgites and the presence of high and low Cr# spinels may be due to the genetic artifact of the different ultramafic units.

Keywords. Spinel peridotites; Nidar Ophiolite Complex (NOC); supra-subduction zone (SSZ); partial melting.

1. Introduction

The *ophiolitic* complexes of the world provide us vital clues in understanding magmatic and tectonic process for the formation of oceanic lithosphere (Ahmed *et al.* 2005) and their emplacement on the margins of continental lithosphere. Ophiolite genesis is in a variety of tectonic settings, either at the suprasubduction zone (SSZ) or mid-ocean ridge (MOR) settings, as shown by refractory mantle character and Cr-rich spinel in peridotites (Pearce *et al.* 1981; Dick and Bullen 1984). Peridotites are the most abundant rock type in *ophiolitic* complexes and are the key sources of geochemical and petrological information of the upper mantle. Phase composition of the *ophiolitic* mantle ultramafic rocks is dependent on the degree and conditions of partial melting and the effects of magma–rock interactions (Uysal *et al.* 2012). Well preserved and fresh peridotite sequence in ophiolite complexes, can be a good source to examine the compositional variations and chemical geodynamics of upper mantle.

The Indus Suture Zone (ISZ) are the remnants of the Neo Tethyan ocean which closed during the Early Cretaceous (110–130 Ma: Mahéo *et al.* 2004: cooling ages; ∼120–110 Ma: Pudsey 1986). It was followed by obduction in Late Cretaceous in

Supplementary materials pertaining to this article are available on the Journal of Earth Science Website (http://www.ias.ac.in/Journals/Journal_of_Earth_System_Science).

Published online: 09 January 2020

Kohistan–Ladakh terranes (Searle *et al.* 1999) as the Indian plate wandered towards the Asian plate (Ahmed *et al.* 2008). An island arc origin was inferred by Thakur and Bhatt (1983) for the volcanic sequence but Ahmed *et al.* (2008) proposed that the mafic unit of Nidar Ophiolite Complex (NOC) is intra-oceanic arc magmatism. Previous studies (Sachan 2001; Siddaiah and Masuda 2001) suggested that the formation of NOC is in a supra subduction zone environment. NOC is a well-exposed Indus Suture Zone Ophiolite complex. The occurrence of high-pressure mineral like clinoenstatite, coesite shows that the peridotites were formed in the mantle transition zone (Das *et al.* 2015). Diamond inclusions were also reported within enstatite and olivine from peridotites of ISZ ophiolite indicating the origin of peridotites at much great depth (∼410 km) (Das *et al.* 2017). The ultramafic rocks of the Nidar ophiolites are remarkably fresh, and the relict primary minerals could be used to infer the original characteristics. In the present study, we have analyzed primary silicate mineral phases of mantle rocks of the Nidar ophiolite to find out the equilibrium condition and related intensive parameter of the mantle-sequence. The study is expected to give insights into the mantle processes (such as partial melting and metasomatism) as well as the tectonic setting of the Nidar ophiolite.

2. Geology of the area

The ISZ is one of the main tectonic units of the northern Himalayas, covering nearly 2500 km from Main Mantle Thrust at Pakistan (Tahirkheli *et al.* 1979; Ahmed *et al.* 2008) in the west to the Lhasa block in the east (Le Fort 1975; Molnar and Tapponnier 1975). The sedimentary and ophiolite sequences are the remnants of the Neo-Tethys seafloor (Thakur and Mishra 1984; Ahmed *et al.* 2008). NOC is a block, thrust over the Indus Group and Ladakh batholith (figure 1) to the north and it has a thrust contact with the Zildat ophiolite mélange in the south (Maheo *et al.* 2004). Further south the Zildat ophiolite mélange has a thrust contact with the Tso Morari Crystalline Complex bearing ultra-high pressure minerals (Mukherjee *et al.* 2003). The general trend of Zildat ophiolite mélange is NW-SE, sandwiched between Tso-Morari Crystalline in the south and the NOC in the north (Sen *et al.* 2013). It consists of serpentine, gabbro, chert, exotic blocks of limestone and clasts of blueschists. The sequences of Nidar ophiolite are well exposed from Nidar village to Kyun Tso, the total thickness of the whole sequence is about 12 km. The ophiolite complex can be divided into three main units from north to south. The ultramafic unit is the basal unit of about 8–10 km in thickness (Sachan 2001), gabbros in the middle and at the top are the volcanic rocks consisting of sheeted dykes and volcanogenic sediments with chert (Ravikant *et al.* 2004; Das *et al.* 2015).

Dunite, peridotite (harzburgite and lherzolite) and pyroxenite veins form the ultramafic unit. Harzburgite is the dominant peridotite. The samples have undergone varying degrees of serpentinization. Dunite is associated with the harzburgite and occurs as lensoidal bodies at few places. The peridotites from NOC is cutting across by discordant dunite sequences in some places and peridotites are also encountered in the field within the channelized dunite (Siddaiah 2001; Sachan and Mukherjee 2003; Das *et al.* 2015). The basal dunite body host podiform chromitite of about 1–1.5 m thick and thin bends of chromitite (Sachan and Mukherjee 2003; Sachan *et al.* 2007). Pyroxenite veins are present in dunite and harzburgite as sills and dykes (Sachan 2001). The gabbroic unit of NOC shows variations from fine grain to coarse grain without any compositional layering. Pillow lava displays a concordant association with the gabbros of the sequence and it is superimposed by volcano-sedimentary unit comprising basaltic to andesitic flows. The lower stratigraphic part of the topmost unit has pillow lavas and it consists of volcanogenic derived intercalated sediments like conglomerates, shale, chert, siltstone and jasperite (Sharma and Gupta 1982).

3. Sampling and field observations

Fresh samples of harzburgite and dunite were collected along the Nidar valley to Kyun Tso. In the study area, the dominant lithology is massive and partially serpentinized harzburgites (∼60%), followed by dunite (∼20%), lherzolite (∼5%) and pyroxenite veins. Undeformed coarse-grained pyroxenite dykes (figure 2a) and dunite veins crosscut the harzburgite (figure 2b) at a few places. Channelized networks of dunite trending NE–SW with disseminated chromite are also encountered (figure 2c). The basal part of the mantle section is marked by the presence of spinel-bearing dunite with moderate serpentinization (Das *et al.* 2015). Here, we attempt to illustrate the petrogenetic processes that could explain the peridotite–dunite association in the studied area.

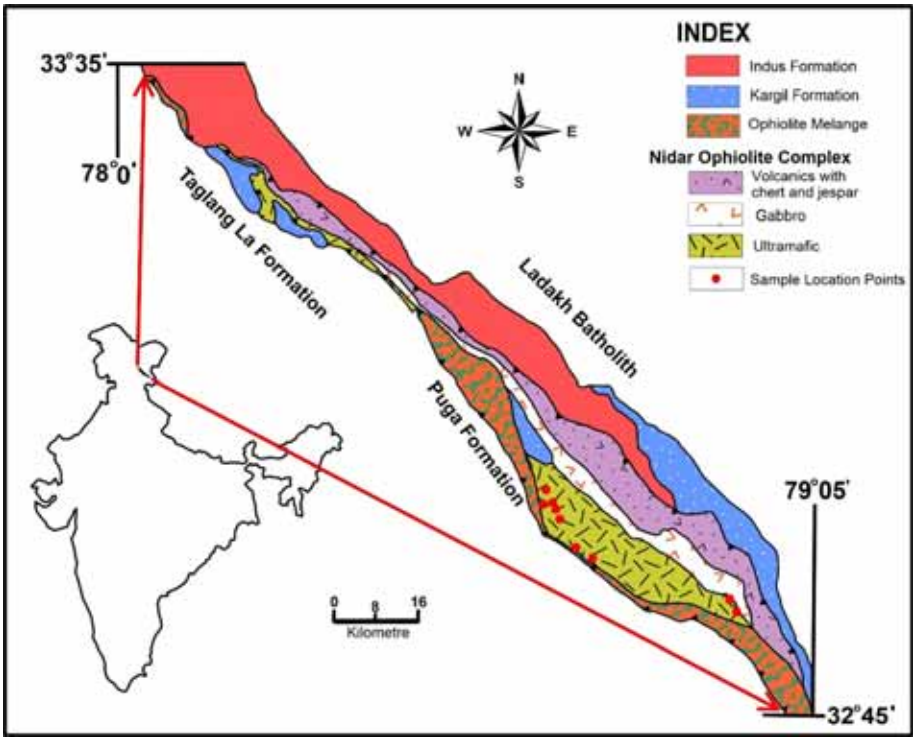

Figure 1. Simplified geological map of Nidar Ophiolite Complex (after Thakur and Misra 1984).

4. Petrography

4.1 *Harzburgite*

Modal composition of harzburgites ranges between 69 and 78% olivine, orthopyroxene varying between 15 and 21%, clinopyroxene from 1 to 3%, and spinel ranging between 1 and 2% and mainly shows protogranular and porphyroclastic texture. In protogranular texture, olivine and orthopyroxene grains display deformation features like kink bands and distorted lamellae in orthopyroxene (figure 3a and b). Recrystallization of olivine around orthopyroxene is observed in harzburgites (figure 3b). Orthopyroxene occurs as large prophyroclasts with exsolutions of clinopyroxene (figure 3b). In some samples, orthopyroxene clasts *host* olivine inclusions (figure 3c). In porphyroclastic type of texture, large orthopyroxene grains form resorbed shapes and small clinopyroxene crystals with lobate boundaries. The occurrence of spinels in harzburgite is in the form of subhedral (figure 3d).

4.2 *Dunite*

Dunites are relatively fresh, modal composition of olivine is about 90%, 5% spinel and a minor amount of pyroxenes. The spinels are more or less euhedral and contain olivine inclusions and also occurs as euhedral to anhedral crystals (figure 3e–g). In some of the sections, spinel occurs as dark red vermicular crystals and occasionally magnetite rim surrounded spinel are also observed (figure 3h).

5. Analytical techniques

Selected samples of harzburgite and dunite were analyzed by a CAMECA SX100 electron microprobe at the Department of Geology and Geophysics, Indian Institute of Technology, Kharagpur (India). Major element compositions of the mineral phases were measured with an accelerating voltage of 15 kV with a beam diameter of 2 μm and probe current of 20 nA. Natural and synthetic standards were used during the analysis. Standards are jadeite (Na-Kα), fluor-apatite (F-Kα, P-Kα), NaCl (Cl-Ka), Fe_2O_3 (Fe-Ka), diopside (Ca-Ka), MgO (Mg-Ka), Al_2O_3 (Al-Ka), rhodonite (Mn-Ka), TiO_2 (Ti-Ka), barite (Ba-La), sphalerite (Zn-Ka), Cr_2O_3 (Cr-Ka). A TAP crystal was used to analyze F, Na, Al, Si, and Mg; PET for Ca, Ti, K, P, Ba and Cl; LIF for Mn, Cr, Zn and Fe. ZAF matrix corrections were performed by the Cameca supplied PAPSIL software. The analyses yielded Mg, Ca, Fe, Cr, Al

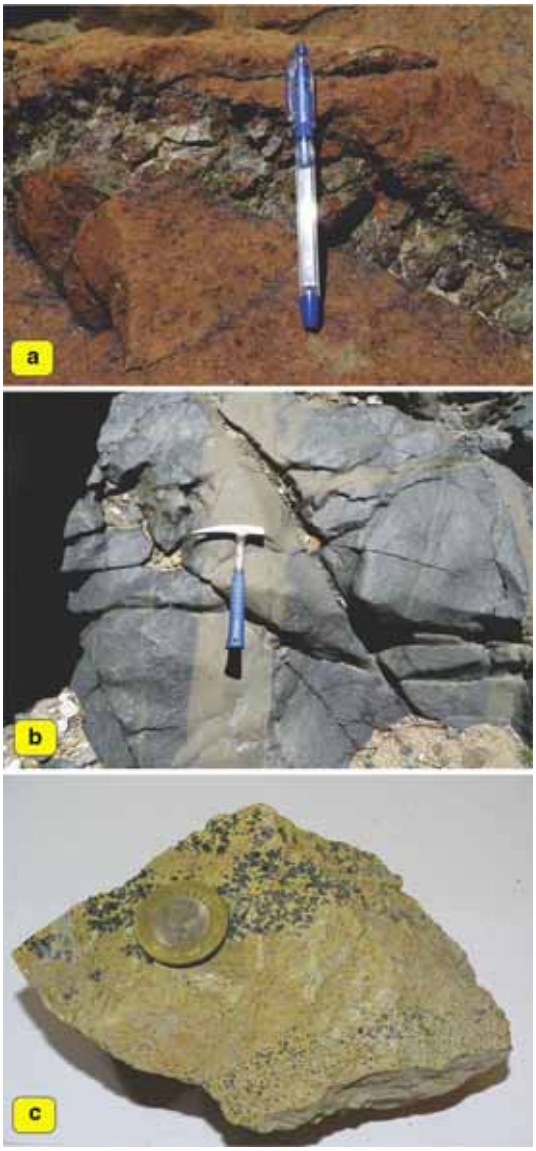

Figure 2. Field photographs of spinel peridotites from basal section of NOC. (**a**) A pyroxenite vein in a massive harzburgite; (**b**) Dunite veins cutting across harzburgite; and (**c**) *Disseminated* and nodular chromitite in dunite.

and Ti contents below detection limits of 336, 552, 1832, 1476, 326 and 664 (ppm), respectively.

6. Mineral chemistry

6.1 *Olivine*

Olivine in harzburgite and dunites of the ophiolite complex show compositionally homogeneous with Fo_{90}–Fo_{92} (table 1 and figure 4). Mg# of olivine in dunite and harzburgite varies from 0.91 to 0.94 and CaO content is <0.06 wt.%. Both the rock types contain low MnO (<0.23 wt.%).

6.2 *Orthopyroxene*

Orthopyroxene in harzburgites is found to be enstatite with $Wo_{1–3}En_{88–91}Fs_{8–9}$ compositions (table 2). The mineral phase contains high CaO (0.40–1.59 wt.%) and Cr_2O_3 (0.43–1.04 wt.%) and Al_2O_3 (0.81–3.75 wt.%). The analyzed grains show variable Mg# from the core (0.96) to rim (0.92).

6.3 *Clinopyroxene*

The CaO content varies from 23.56 to 25.28 wt.% and the Cr_2O_3 between 0.12 to 1.57 wt.%. TiO_2 (<0.16 wt.%) content in clinopyroxene is low. Core-rim compositional profile shows the CaO content increases, whereas the Al_2O_3 and Cr_2O_3 content decreases. The studied clinopyroxene from NOC is TiO_2 and Na_2O deficient diopside (table 3).

6.4 *Chromian spinel*

Chromian spinels of harzburgites and dunites were analyzed (table 4). The analyzed spinel in harzburgite show variable Cr_2O_3 (23.50 to 55.44 wt.%). Chromian spinels of the studied ultramafic rocks shows variable Al_2O_3 (14.29–44.97 wt.% for the harzburgite and 7.35–15.60 wt.% in dunite). Chromian spinel in harzburgites is found to be magnesiochromite and variable Cr# [Cr/(Cr+Al)] 0.26 to 0.72. Low TiO_2 (<0.12 wt.%) content of the spinels show the residual nature of the samples. MnO content is low (<0.35 wt.%). Mg# ranges between 0.45 to 0.72 and Fe^{3+}# [Fe^{3+}/(Fe^{3+}+ Cr+Al)] is low (<0.04) and display no major variation in harzburgites.

7. Discussion

7.1 *Partial melting*

Several studies have been carried out by petrologists to determine the tectonic settings of ultramafic rocks based on the composition of the mineral phases (Jan and Windley 1990; Arai 1994a; Monnier *et al.* 1995; Franz and Wirth 2000; Kamenetsky *et al.* 2001). Particularly, Cr-spinel is used for the petrological characterization and to have an *idea* about the tectonic setting of the ophiolite complexes. Chromian spinels can survive metamorphism and it is a dependable key mineral of the primary mantle lithology or in the altered

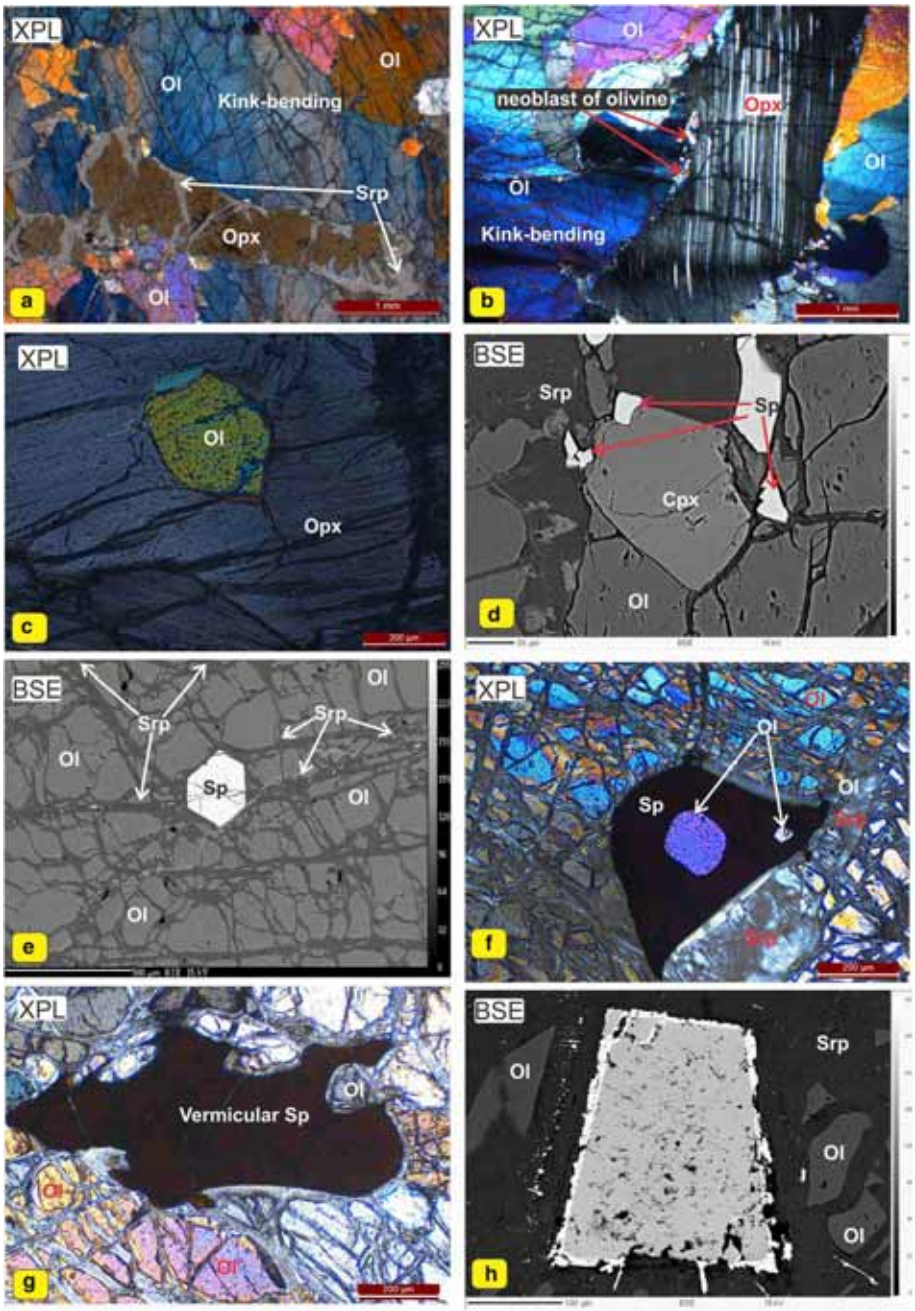

Figure 3. Photomicrographs of the studied spinel peridotites and dunites: (**a**) Olivine grains showing *kink-bending* and partial *serpentinisation* of orthopyroxene in harzburgite; (**b**) Porphyroclastic orthopyroxene exhibiting distorted lamellae with exsolution of clinopyroxene; (**c**) Olivine inclusion in orthopyroxene; (**d**) Subhedral grains of spinel and primary clinopyroxene; (**e**) Euhedral spinel and partial, altered and wrapped; (**f**) Olivine inclusions in spinel, wrapped in highly fractured olivine as observed in dunite; (**g**) Olivine embayment and vermicular spinel; and (**h**) Partially altered spinel with higher concentration of Iron at the grain boundary and high concentration of Chromium at the core is observed in harzburgite. (Ol: olivine, Opx: orthopyroxene, Cpx: clinopyroxene, Srp: serpentine, Sp: Cr spinel).

ultramafic rocks (Liipo *et al.* 1995). Possibly, depending on the tectonic setting, there will be differences in the degree of melting of peridotite (Dick and Bullen 1984; Arai 1994b). Petrogenesis of dunites in ophiolite is very complex and is known to be a multi-stage process (Zhou *et al.* 2005). Peridotites from NOC exhibit a depleted character in terms of mineralogy and mineral chemistry and may be the residues of high degree of partial melting as it has low Na_2O and K_2O content (<0.23 and <0.04 wt.%, respectively) in clinopyroxene, which suggests the depleted nature of the rocks (Kapsiotis 2014). Mineral chemistry of peridotites reveals a multi-stage genesis. Evidence of high

Table 1. *Representative electron microprobe analyses of olivine in harzburgite and dunite of NOC, Ladakh Himalaya.*

	Harzburgite												Dunite			
Sample no.	40	40/1	41	41/1	45	45/1	76	76/1	80	80/1	92	92/1	44	44/1	97	97/1
SiO_2	40.88	40.52	40.60	40.38	40.43	40.24	40.60	40.70	40.08	40.99	40.09	40.62	40.91	40.98	40.68	40.82
TiO_2	0.00	0.00	0.00	0.02	0.00	0.00	0.00	0.00	0.00	0.00	0.00	0.00	0.00	0.00	0.03	0.00
Al_2O_3	0.00	0.02	0.00	0.04	0.01	0.01	0.03	0.00	0.00	0.00	0.00	0.00	0.00	0.00	0.01	0.02
Cr_2O_3	0.00	0.02	0.00	0.04	0.00	0.05	0.04	0.00	0.00	0.09	0.03	0.06	0.02	0.00	0.00	0.00
FeO	8.64	9.17	8.87	9.12	9.29	8.82	9.43	8.87	9.03	8.10	8.93	9.52	8.08	8.05	7.26	7.59
MnO	0.12	0.23	0.13	0.04	0.21	0.19	0.17	0.12	0.07	0.06	0.10	0.19	0.06	0.04	0.20	0.14
MgO	50.62	50.01	50.28	50.30	50.05	50.65	49.67	50.41	50.73	50.69	50.65	49.50	50.84	50.85	51.77	51.35
CaO	0.05	0.00	0.04	0.00	0.01	0.04	0.06	0.02	0.03	0.02	0.02	0.06	0.06	0.00	0.05	0.06
Na_2O	0.04	0.03	0.03	0.03	0.00	0.00	0.00	0.00	0.03	0.04	0.01	0.03	0.01	0.05	0.00	0.00
K_2O	0.00	0.00	0.04	0.01	0.00	0.01	0.00	0.00	0.00	0.00	0.02	0.01	0.00	0.02	0.00	0.02
Total	100.42	100.00	100.00	99.98	99.99	100.00	100.00	100.12	99.96	100.00	99.85	100.00	99.97	100.00	99.99	100.00
Si	0.991	0.988	0.989	0.984	0.986	0.979	0.992	0.990	0.975	0.996	0.976	0.994	0.993	0.995	0.983	0.988
Ti	0.000	0.000	0.000	0.000	0.000	0.000	0.000	0.000	0.000	0.000	0.000	0.000	0.000	0.000	0.001	0.000
Al	0.000	0.001	0.000	0.001	0.000	0.000	0.001	0.000	0.000	0.000	0.000	0.000	0.000	0.000	0.000	0.001
Cr	0.000	0.000	0.000	0.001	0.000	0.001	0.001	0.000	0.000	0.002	0.001	0.001	0.000	0.000	0.000	0.000
Fe^{3+}	0.018	0.022	0.022	0.029	0.027	0.042	0.012	0.021	0.050	0.006	0.047	0.012	0.014	0.010	0.033	0.023
Fe^{2+}	0.158	0.165	0.159	0.157	0.162	0.138	0.180	0.159	0.133	0.158	0.135	0.183	0.150	0.154	0.114	0.131
Mn	0.002	0.005	0.003	0.001	0.004	0.004	0.004	0.003	0.001	0.001	0.002	0.004	0.001	0.001	0.004	0.003
Mg	1.830	1.819	1.826	1.827	1.820	1.836	1.809	1.827	1.840	1.836	1.839	1.805	1.840	1.841	1.865	1.853
Ca	0.001	0.000	0.001	0.000	0.000	0.001	0.002	0.001	0.001	0.001	0.001	0.002	0.002	0.000	0.001	0.001
Mg#	0.921	0.917	0.920	0.921	0.918	0.930	0.910	0.920	0.933	0.921	0.932	0.908	0.925	0.923	0.942	0.934
Te	0.120	0.240	0.130	0.040	0.220	0.190	0.180	0.120	0.070	0.060	0.100	0.200	0.060	0.040	0.190	0.140
Fo	91.090	90.460	90.820	90.740	90.370	90.880	90.150	90.880	90.830	91.690	90.880	90.010	91.690	91.810	92.480	92.150
Fa	8.720	9.300	8.990	9.230	9.410	8.880	9.590	8.970	9.060	8.230	8.990	9.700	8.170	8.150	7.270	7.640

Mg#: $Mg/(Mg+Fe^{2+})$.

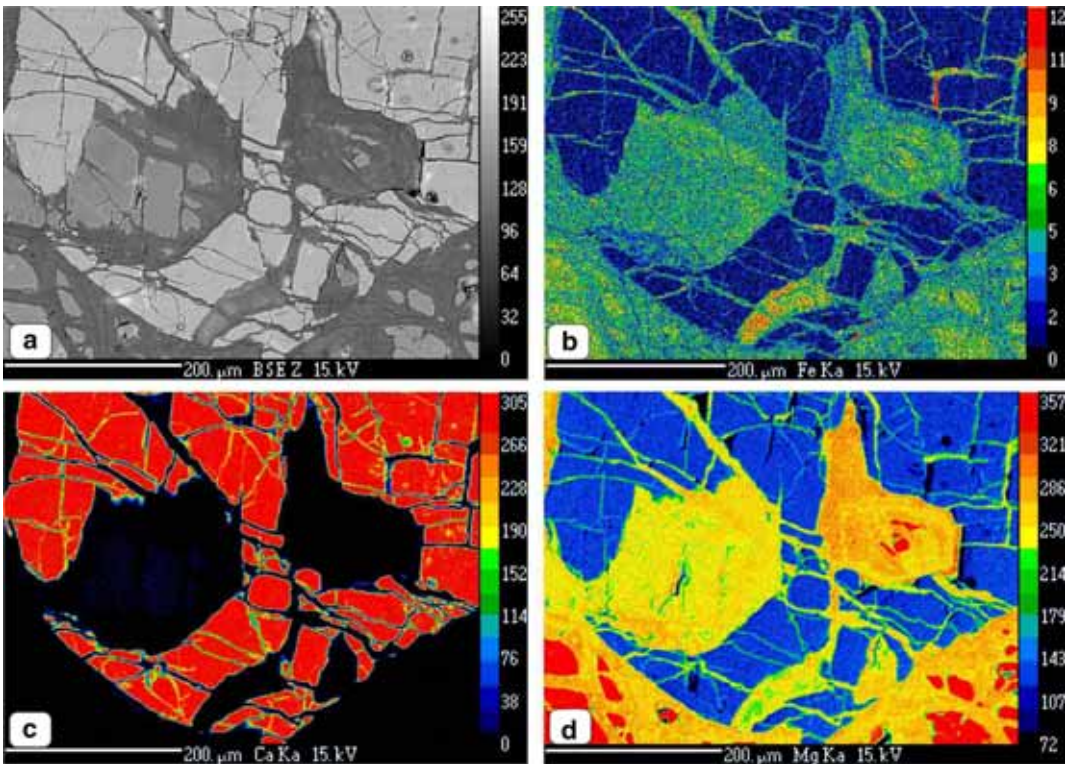

Figure 4. Back scattered electron image of porphyroclastic clinopyroxene and olivine (**a**) and elemental mapping images of olivine and clinopyroxene mineral (**b–d**).

degree of partial melting can be inferred from low modal composition of clinopyroxene in harzburgites (<4 vol.%), high fosterite content (Fo_{90}) in olivine, pyroxene showing low Al_2O_3 (avg. 2.16 wt.% for orthopyroxene and 1.82 for clinopyroxene) and wide range of Cr# values (0.26–0.72) (Coish and Gardner 2004; Khalil and Azer 2008; Kapsiotis 2016). Depleted nature of peridotites is in agreement with the depletion of incompatible elements like Na and Ti in pyroxenes akin to the arc peridotites (Ishii *et al.* 1992; Pearce *et al.* 2000). In general, chromian spinels in dunites show higher Cr# values (>0.7) (Godard *et al.* 2008; Uysal *et al.* 2012). In the studied samples, spinels from dunite show higher Cr# (0.69-0.85), low MgO and higher FeO content than those of harzburgites spinels (table 4) and may suggest different petrogenesis of the studied ultramafic rocks.

Chromian spinel compositions are useful to indicate that the mantle peridotites have undergone the degree of partial melting (Dick and Bullen 1984; Arai 1992; Zhou *et al.* 1998; Hellebrand *et al.* 2001; Kamenetsky *et al.* 2001; Zhou *et al.* 2005; Okamura *et al.* 2006; Uysal *et al.* 2007; Bédard *et al.* 2009; Gonzalez-Jimenez *et al.* 2011). The olivine spinel mantle array (OSMA) diagram of Arai (1992) is widely used to describe mantle-derived, spinel-bearing peridotites based on the trend of melting for a fertile MORB mantle. The plot of Cr spinel *vs.* olivine (figure 5) indicates that the harzburgites were formed due to partial melting of around 10–38% (FMM: fertile MORB mantle). The considerable difference in the peridotite (harzburgite and dunite) is reflected in variable Cr# (0.26–0.85) in Cr spinel. Studies have shown the distinct relationship between the Cr# of Cr spinels and degree of partial melting in mantle relicts of ophiolites or abyssal peridotites (e.g., Dick and Bullen 1984; Batanova *et al.* 1998; Hellebrand *et al.* 2002). Both orthopyroxene and clinopyroxene are rich in MgO and the plot of Al_2O_3 wt.% in pyroxenes *vs.* Cr#s of the coexisting spinel of the restitic peridotite follows a depletion trend (figure 6).

7.2 *Melt–rock interaction*

Although harzburgite is considered as depleted, refractory residues of partially melted mantle components (Himmelberg and Loney 1973), observations in the field and petrographical features of the NOC harzburgites indicates melt–rock interactions. Harzburgite hosting dunite enclave can explain the interaction of infiltrating melts and

Table 2. *Representative electron microprobe analyses of orthopyroxene in harzburgite of NOC, Ladakh Himalaya.*

	Harzburgite											
Sample no.	40	40/1	41	41/1	45	45/1	76	76/1	80	80/1	92	92/1
SiO_2	56.83	56.66	56.39	56.63	55.13	55.58	55.45	55.82	56.15	56.36	55.01	55.43
TiO_2	0.00	0.00	0.00	0.00	0.04	0.00	0.02	0.02	0.00	0.00	0.01	0.02
Al_2O_3	1.83	1.90	1.50	0.81	2.44	2.40	2.32	2.16	1.50	1.68	3.75	3.70
Cr_2O_3	0.58	0.65	0.43	0.91	0.67	0.64	0.81	0.54	0.57	0.67	0.68	1.04
FeO	5.51	5.21	5.73	5.85	5.90	6.24	6.09	6.38	6.00	5.77	6.15	5.77
MnO	0.08	0.21	0.12	0.13	0.12	0.12	0.06	0.17	0.11	0.12	0.16	0.16
MgO	34.09	34.12	34.56	35.30	34.80	33.67	34.40	34.34	34.64	34.95	33.49	33.61
CaO	1.05	1.26	1.32	0.46	0.92	1.59	0.84	0.55	0.92	0.40	0.69	0.56
Na_2O	0.07	0.00	0.04	0.00	0.00	0.00	0.02	0.02	0.00	0.02	0.02	0.00
K_2O	0.00	0.02	0.00	0.00	0.00	0.00	0.01	0.00	0.00	0.00	0.02	0.00
Total	100.04	100.02	100.08	100.08	100.02	100.24	100.01	100.02	99.91	99.97	99.99	100.27
Si	1.956	1.951	1.938	1.946	1.894	1.914	1.909	1.923	1.936	1.937	1.897	1.907
Ti	0.000	0.000	0.000	0.000	0.001	0.000	0.000	0.000	0.000	0.000	0.000	0.000
Al	0.074	0.077	0.061	0.033	0.099	0.097	0.094	0.088	0.061	0.069	0.152	0.150
Cr	0.016	0.018	0.012	0.025	0.018	0.017	0.022	0.015	0.015	0.018	0.019	0.028
Fe^{3+}	0.002	0.003	0.054	0.051	0.094	0.057	0.066	0.051	0.051	0.040	0.035	0.007
Fe^{2+}	0.157	0.148	0.110	0.117	0.076	0.123	0.109	0.132	0.122	0.126	0.142	0.158
Mn	0.002	0.006	0.003	0.004	0.003	0.003	0.002	0.005	0.003	0.004	0.005	0.005
Mg	1.749	1.751	1.770	1.808	1.782	1.729	1.765	1.764	1.777	1.790	1.722	1.724
Ca	0.039	0.046	0.049	0.017	0.034	0.059	0.031	0.020	0.034	0.015	0.026	0.021
Na	0.005	0.000	0.002	0.000	0.000	0.000	0.001	0.001	0.000	0.001	0.001	0.000
Mg#	0.918	0.922	0.941	0.939	0.959	0.934	0.942	0.930	0.936	0.934	0.924	0.916
Cr#	0.178	0.189	0.164	0.431	0.154	0.149	0.190	0.146	0.197	0.207	0.111	0.157
Wo	1.990	2.380	2.450	0.850	1.690	2.980	1.570	1.010	1.700	0.760	1.330	1.070
En	89.860	89.910	89.250	90.720	89.780	87.880	89.540	89.650	89.590	90.830	89.450	90.240
Fs	8.150	7.710	8.300	8.430	8.530	9.130	8.890	9.340	8.710	8.410	9.210	8.680

Mg#: $Mg/(Mg+Fe^{2+})$; Cr#: Cr/(Cr+Al).

upper mantle peridotites (Edwards and Malpas 1995). The pyroxene porphyroclast displaying corroded margins filled with olivine (figure 3c) and minor Cr spinel neoblasts resulted due to the dissolution of orthopyroxene and olivine precipitation by a melt of undersaturated pyroxene (Kelemen 1990; Dijkstra *et al.* 2003; Parkinson Kapsiotis 2016). The studied samples show textural features indicating melt–rock interactions like olivine as inclusions in the spinel (figure 3d) and olivine embayments (figure 3g) partly corroding the orthopyroxene porphyroclast (Bédard *et al.* 2009; Dilek and Morishita 2009; Hellebrand *et al.* 2002; Zhou *et al.* 2005). In harzburgite, a minor amount of clinopyroxene might have *subsolidus* origin due to decomposition of high-T orthopyroxene on cooling and it appears as exsolution lamellae in orthopyroxene (figure 3b) or as small separate interstitial grains between orthopyroxene and olivine clasts (Peighambari *et al.* 2011; Moghadam *et al.* 2015). If the peridotite-melt reaction occurred at a temperature lower than peridotite solidus, the significant decrease of the modal volume of orthopyroxene in dunite requires that the melt was undersaturated (Sachan 2001).

Previous studies have suggested that the petrogenesis of the dunite veins and dykes associated with ophiolite mantle sections are produced by high degrees of partial melting (e.g., Mysen and Kushiro 1977; Nicolas 1989). The distinct dunite band with well-defined margins suggests *that* intrusion of magma into a fracture and subsequent cooling and crystallization. The constant forsterite composition in dunite suggests that the intruding magma retained a nearly constant composition and might have injected uninterruptedly through the dikes. Dunite may also be produced from incongruent dissolution of pyroxene through a reaction in between tholeiitic melt and peridotite (Kelemen 1990). If the *in-situ* partial melting of peridotite leading to the formation of dunite, it can be expected that the magnesian content in

Table 3. *Representative electron microprobe analyses of clinopyroxene in harzburgite of NOC, Ladakh Himalaya.*

	Harzburgite											
Sample no.	40	40/1	41	41/1	45	45/1	76	76/1	80	80/1	92	92/1
SiO_2	53.96	52.91	53.20	53.64	50.75	52.52	53.81	53.70	52.80	52.86	51.32	51.67
TiO_2	0.00	0.00	0.06	0.00	0.04	0.06	0.05	0.02	0.00	0.01	0.16	0.08
Al_2O_3	1.77	1.79	1.19	0.91	3.69	2.17	1.16	0.89	1.61	1.54	3.73	3.18
Cr_2O_3	0.94	0.82	0.76	0.56	1.57	0.71	0.12	0.20	0.79	1.01	1.07	0.72
FeO	1.47	1.52	1.80	1.40	2.70	1.70	1.95	1.69	1.73	1.58	1.90	2.32
MnO	0.00	0.14	0.04	0.08	0.13	0.18	0.06	0.12	0.21	0.10	0.04	0.12
MgO	17.64	17.67	17.97	18.13	17.30	17.10	18.11	18.54	17.85	17.71	17.35	16.99
CaO	24.21	25.01	24.97	25.22	23.56	25.28	24.51	24.70	24.39	24.85	24.28	24.68
Na_2O	0.01	0.09	0.05	0.07	0.05	0.05	0.08	0.06	0.23	0.15	0.10	0.04
K_2O	0.02	0.00	0.01	0.01	0.00	0.02	0.01	0.02	0.02	0.04	0.00	0.00
Total	100.01	99.94	100.07	100.01	99.92	99.85	99.97	99.97	99.71	99.90	100.01	99.80
Si	1.957	1.918	1.927	1.941	1.848	1.911	1.950	1.941	1.918	1.919	1.860	1.880
Ti	0.000	0.000	0.002	0.000	0.001	0.002	0.001	0.001	0.000	0.000	0.004	0.002
Al	0.076	0.076	0.051	0.039	0.158	0.093	0.049	0.038	0.069	0.066	0.159	0.136
Cr	0.027	0.024	0.022	0.016	0.045	0.020	0.003	0.006	0.023	0.029	0.031	0.021
Fe^{3+}	0.000	0.046	0.055	0.042	0.000	0.000	0.008	0.000	0.000	0.000	0.058	0.071
Fe^{2+}	0.045	0.000	0.000	0.000	0.082	0.052	0.059	0.051	0.053	0.048	0.000	0.000
Mn	0.000	0.004	0.001	0.002	0.004	0.006	0.002	0.004	0.007	0.003	0.001	0.004
Mg	0.954	0.955	0.970	0.978	0.939	0.928	0.978	0.999	0.966	0.958	0.937	0.922
Ca	0.941	0.971	0.969	0.978	0.919	0.985	0.951	0.956	0.949	0.966	0.943	0.962
Na	0.001	0.006	0.004	0.005	0.004	0.004	0.006	0.004	0.016	0.011	0.007	0.003
Mg#	0.955	0.954	0.946	0.959	0.920	0.947	0.936	0.951	0.948	0.952	0.942	0.928
Cr#	0.262	0.240	0.301	0.291	0.222	0.177	0.058	0.136	0.250	0.305	0.163	0.134
Wo	48.520	49.250	48.600	48.940	47.360	50.150	47.840	47.670	48.220	48.980	48.660	49.220
En	49.180	48.410	48.660	48.940	48.400	47.210	49.180	49.790	49.110	48.590	48.370	47.160
Fs	2.300	2.330	2.740	2.120	4.240	2.640	2.980	2.540	2.670	2.430	2.970	3.620

Mg#: $Mg/(Mg+Fe^{2+})$; Cr#: Cr/(Cr+Al).

olivine of dunite will be higher than olivine of harzburgite. In other words, if the dunite bodies were produced by fractional crystallization from picritic magma, then there will be a trend of iron enrichment in olivine of dunite and the compositional range will be much higher in olivine of dunite than in olivine of harzburgite. In the present study, the composition of olivine in harzburgite and dunite (table 1) do not show significant variations indicating that partial melting is the dominant process in the formation of peridotites in Nidar ophiolite.

7.3 *Tectonic setting*

The mineral chemistry of mantle relics is supposed to reveal the difference of the melting regimes in various tectonic settings. The primary mineral phase composition in peridotites is considered as a powerful petrogenetic tool and can be used to infer their tectonic setting (Hebert *et al.* 2003; Bédard *et al.* 2009). The present work involves the detailed study of chromian spinels of peridotites from Nidar ophiolite. In the plot (figure 7) Mg# and Cr# of Cr spinel fall in the forearc peridotite field (Juteau *et al.* 1990; Ohara and Ishii 1998 and references therein) and few samples overlap in the field of abyssal peridotites. Spinel Cr# *vs.* olivine Mg# diagram shows NOC samples belongs to both intra-oceanic subduction zone peridotites and abyssal peridotites (Dick and Bullen 1984; Pearce *et al.* 2000). The Cr_2O_3 in orthopyroxene (wt.%) *vs.* Al_2O_3 in clinopyroxene (wt.%) diagram in figure 8 show that majority of the NOC peridotite belongs to forearc peridotite and only a few belong to abyssal peridotite. These observations are in accordance with the earlier results reported by Johnson *et al.* (1990), Juteau *et al.* (1990) and Ishii *et al.* (1992). In the Cr# *vs.* TiO_2 wt.% diagram studied peridotite belongs to both arc and MOR settings (figure 9). Petrological and geochemical data from ophiolitic and abyssal peridotites have

Table 4. *Representative electron microprobe analyses of spinel in harzburgite and dunite of NOC, Ladakh Himalaya.*

	Harzburgite												Dunite			
Sample no.	40	40/1	41	41/1	45	45/1	76	76/1	80	80/1	92	92/1	44	44/1	97	97/1
SiO_2	0.07	0.09	0.04	0.00	0.00	0.01	0.02	0.01	0.04	0.00	0.00	0.04	0.08	0.03	0.03	0.01
TiO_2	0.07	0.03	0.02	0.00	0.05	0.02	0.00	0.00	0.10	0.12	0.02	0.00	0.13	0.13	0.19	0.19
Al_2O_3	27.28	14.29	18.45	18.45	32.44	33.40	33.27	25.45	20.52	19.64	44.97	42.33	7.35	8.74	15.36	15.17
Cr_2O_3	41.97	55.15	50.59	50.55	34.39	32.72	33.48	42.60	47.83	48.49	23.22	25.67	60.05	59.52	51.85	50.94
FeO	17.90	20.97	19.12	19.64	18.39	20.24	18.51	19.68	19.90	20.15	14.02	14.50	23.11	21.48	20.80	22.74
MnO	0.27	0.18	0.35	0.19	0.15	0.23	0.08	0.31	0.31	0.23	0.18	0.15	0.48	0.28	0.35	0.24
MgO	12.28	9.17	11.41	11.08	14.55	12.70	14.13	11.96	11.31	11.36	17.59	16.96	8.62	9.70	11.32	10.70
CaO	0.11	0.05	0.00	0.02	0.01	0.02	0.02	0.00	0.00	0.00	0.00	0.02	0.00	0.02	0.03	0.01
Na_2O	0.05	0.07	0.02	0.07	0.01	0.02	0.02	0.00	0.00	0.02	0.00	0.00	0.14	0.09	0.06	0.02
K_2O	0.00	0.00	0.00	0.00	0.01	0.00	0.00	0.00	0.00	0.00	0.00	0.02	0.04	0.00	0.00	0.00
Total	99.99	100.00	100.00	100.00	100.00	99.36	99.53	100.01	100.01	100.01	100.00	99.69	99.99	99.99	100.00	100.01
Si	0.002	0.003	0.001	0.000	0.000	0.000	0.001	0.000	0.001	0.000	0.000	0.001	0.003	0.001	0.001	0.000
Ti	0.002	0.001	0.001	0.000	0.001	0.000	0.000	0.000	0.002	0.003	0.000	0.000	0.003	0.003	0.005	0.005
Al	0.975	0.550	0.686	0.688	0.795	1.166	1.150	0.916	0.757	0.727	1.452	1.389	0.292	0.343	0.579	0.574
Cr	1.006	1.423	1.262	1.265	1.117	0.766	0.776	1.029	1.183	1.204	0.503	0.565	1.602	1.566	1.311	1.293
Fe^{3+}	0.012	0.020	0.049	0.047	0.086	0.067	0.073	0.055	0.053	0.064	0.043	0.044	0.093	0.083	0.100	0.124
Fe^{2+}	0.442	0.552	0.456	0.472	0.363	0.434	0.381	0.448	0.468	0.465	0.278	0.293	0.559	0.515	0.457	0.487
Mn	0.007	0.005	0.009	0.005	0.004	0.006	0.002	0.008	0.008	0.006	0.004	0.004	0.014	0.008	0.009	0.007
Mg	0.555	0.447	0.537	0.523	0.634	0.561	0.618	0.545	0.528	0.532	0.719	0.704	0.434	0.481	0.539	0.512
Cr#	0.508	0.721	0.648	0.648	0.584	0.396	0.403	0.529	0.610	0.624	0.257	0.289	0.846	0.820	0.694	0.693
Fe#	0.012	0.014	0.037	0.036	0.071	0.080	0.086	0.051	0.043	0.050	0.079	0.070	0.055	0.050	0.071	0.088
Mg#	0.553	0.447	0.535	0.541	0.620	0.636	0.609	0.619	0.534	0.542	0.708	0.721	0.437	0.453	0.541	0.513

Mg#: $Mg/(Mg+Fe^{2+})$; Cr#: Cr/(Cr+Al); Fe#: $Fe^{2+}/(Mg+ Fe^{2+})$.

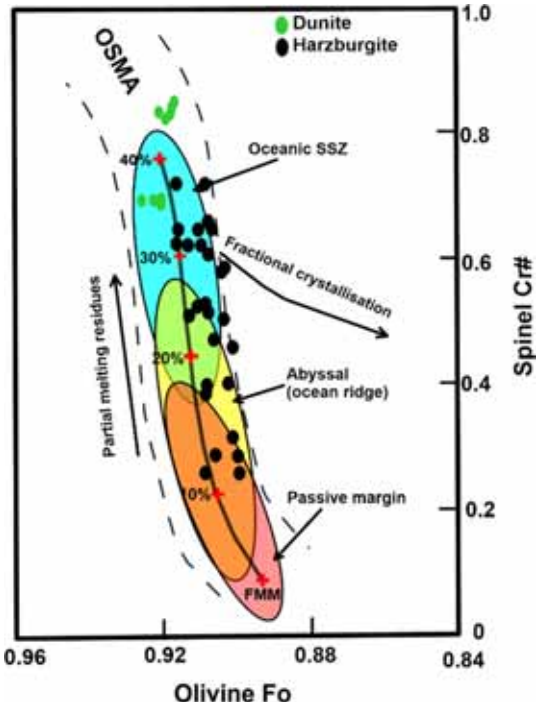

Figure 5. The compositional relationship between Cr# of spinel and Mg# of olivine in harzburgite and dunite from NOC. The olivine–spinel mantle array (OSMA) and the melting trend are from Arai (1994a). FMM: fertile MORB mantle. The bottom ellipse respresents peridotites from passive continental margin (Pearce *et al.* 2000), the middle ellipse is the field for abyssal (ocean ridge) peridotites (Dick and Bullen 1984) and the top ellipse is for supra-subduction peridotites (Ishii *et al.* 1992; Parkinson and Preace 1998). Plot shows that the investgated peridotites fall both in the abyssal peridotites field and the oceanic supra-subduction peridotite field.

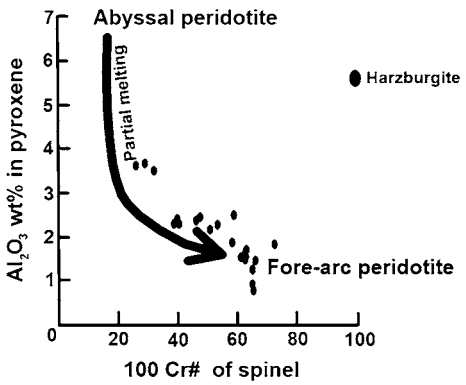

Figure 6. Plot of Al_2O_3 wt.% in pyroxene and Cr# in spinel harzburgite from NOC showing depletion trend.

yielded new ideas into our understanding of variation in the composition of the upper mantle due to varying degrees of partial melting (Niu *et al.* 1997; Takazawa *et al.* 2000; Choi *et al.* 2008; Dilek and Morishita, 2009). But, partial melting cannot be considered the only reason of mantle heterogeneity;

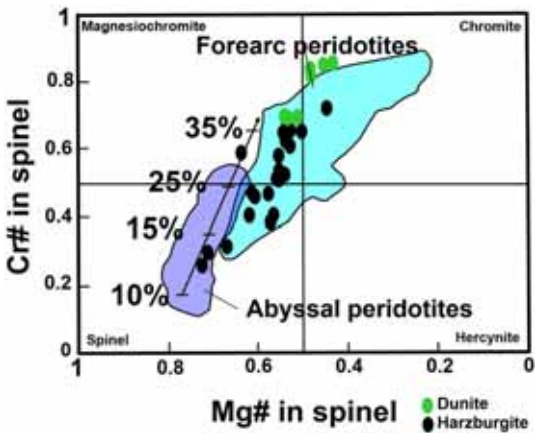

Figure 7. Spinel composition of Nidar ophiolite peridotites. The field for forearc peridotites is from Ishii *et al.* (1992) and Ohara and Ishii (1998). The field for abyssal peridotites is from Dick and Bullen (1984) and Juteau *et al.* (1990). Representation of the degree of partial melting of the parental peridotites as estimated from *experimental* studies (Hiose and Kawamoto 1995).

melt–rock interaction can also lead to significant chemical heterogeneity in the mantle (Kelemen *et al.* 1992; Zhou *et al.* 2005; Uysal *et al.* 2007; Bodinier *et al.* 2008; Choi *et al.* 2008; Rampone *et al.* 2008; Aldanmaz *et al.* 2009; Hanghøj *et al.* 2010).

7.4 *Equilibrium condition*

Equilibrium pressure and temperature condition under which the ultramafic rocks formed, provides information about the nature of the evolution of the *ophiolitic* mantle sequence. The compositions of olivine, orthopyroxene, clinopyroxene, and chromian spinel have been used to establish the crystallization condition of Nidar peridotites and

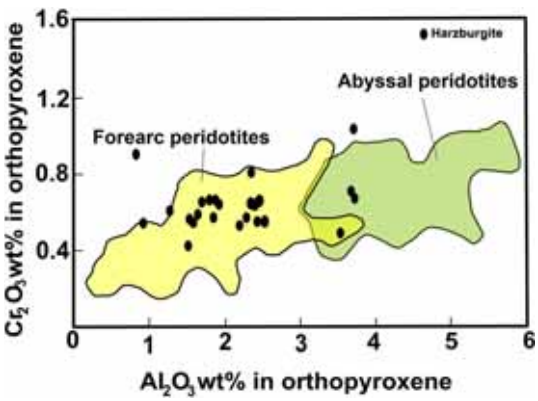

Figure 8. Plot of Al_2O_3 and Cr_2O_3 (wt.%) of orthopyroxenes from Nidar ophiolite peridotites. The abyssal peridotites field from Johnson *et al.* (1990) and Juteau *et al.* (1990); the forarc field is from Ishii *et al.* (1992).

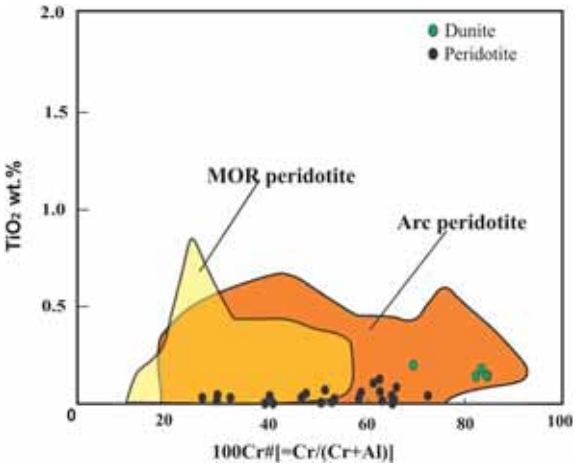

Figure 9. Plot of TiO_2 (wt.%) *vs.* Cr# in Cr-spinel compositions. The compositional fields are from Arai *et al.* (2011).

also to understand the paleogeodynamic setting of the ophiolite complex and probable melt–rock interaction that resulted in the dunite–peridotite association. Various geothermobarometers have been used to estimate the equilibrium parameter of the studied NOC samples. We have used phase chemistry of the co-existing mineral assemblages of the ultramafic rocks and used various geothermobarometric equations to calculate the equilibrium pressure and temperature of the studied ultramafic rocks. Fabries's (1979) spinel–olivine geothermometer was used to calculate an equilibrium temperature within the range 800–900°C. A single clinopyroxene barometer by Nimis and Taylor (2000) was used for the estimation of pressure. The studied samples from Nidar ophiolite exhibits pressure ranging from 32 to 40 kbar.

Oxygen fugacity (fO_2) is important but a less known intensive variable in mantle processes (Ballhaus *et al.* 1991). It affects the pressure–temperature condition of mantle solidus, the composition of the melt and fluids from the mantle, limits the mantle-core equilibria and affects geophysical parameters of the mantle (Green *et al.* 1987; Taylor and Green 1988; Haggerty 1989). The oxygen barometer is valid for the whole range of spinel compositions found in mantle rocks and mantle-derived melts (Ballhaus *et al.* 1991). Oxygen fugacity in this study was estimated using the Ballhaus, Berry and Green equation (1990, 1991). The present samples are found to have equilibrated between −0.09 and 0.55 log units above the FMQ buffer. Differences in the estimated fO_2 value suggested that there are variations in the oxidation of the melts, which are equilibrated with the studied samples. Calculated equilibrium parameters suggest that the studied NOC peridotites have equilibrated in the upper mantle conditions.

8. Conclusion

The petrological study of the ultramafic rocks of the NOC may be summarized as follows:

- Field and petrographical evidence indicates melt–rock interactions during the harzburgite formation.
- Presence of high and low Cr# spinels in the ultramafites (harzburgite and dunite) may be due to petrogenetic activity of the different ultramafic units.
- Mantle section of NOC is composed mainly of highly depleted harzburgite with variable Cr# molar ratio and spinel of the associated dunites contains high Cr# with very low TiO_2 (<0.19 wt.%).
- The rocks have been equilibrated at a temperature of 800–900°C, 32–40 kbar pressure and oxygen fugacity between –0.09 to 0.55 log units above the FMQ buffer.
- Rocks have undergone a high degree of partial melting (between 10–38%).
- The peridotites belong to both intra-oceanic subduction zone and abyssal peridotite.

Supplementary data associated with this article (mineral chemistry of olivine, orthopyroxene, clinopyroxene and spinel (S1–S4)) is given in four different excel sheets.

Acknowledgements

RN acknowledges financial support from the Department of Science and Technology, Government of India as Fast Track Young Scientist (Grant no. SR/FTP/ES-60/2014). RN gratefully acknowledges Dr Stenzin and his family for all the help and support during the fieldwork at Ladakh. Also grateful to Dr C P Dorjey for the logistics during the fieldwork. The author is thankful to Dr Sakthi Saravanan Chinnasamy for extending his Lab facilities for the execution of the DST project. The manuscript is greatly improved from the thoughtful comments by the anonymous reviewers of the journal and language improvement by Akmaz. The author is indebted to Prof Rajneesh

Bhutani, for valuable suggestions and editorial handling.

References

Ahmed A H, Arai S, Abdel-Aziz Y M and Rahimi A 2005 Spinel composition as a petrogenetic indicator of the mantle section in the Neoproterozoic Bou Azzer ophiolite, Anti-Atlas, Morocco; *Precamb. Res.* **138**(**3–4**) 225–234.

Ahmad T, Tanaka T, Sachan H K, Asahara Y, Islam R and Khanna P P 2008 Geochemical and isotopic constraints on the age and origin of the Nidar Ophiolitic Complex, Ladakh, India: Implications for the Neo-Tethyan subduction along the Indus suture zone; *Tectonophys.* **451** 206–224.

Aldanmaz E, Schmidt M W, Gourgaud A and Meisel T 2009 Mid-ocean ridge and supra-subduction geochemical signatures in spinel-peridotites from the Neotethyan ophiolites in SW Turkey: Implications for upper mantle melting processes; *Lithos* **113** 691–708, https://doi.org/10.1016/j.lithos.2009.03.010.

Arai S 1992 Chemistry of chromian spinel in volcanic rocks as a potential guide to magma chemistry; *Mineral. Mag.* **56** 173–184.

Arai S 1994a Compositional variation of olivine-chromian spinel in Mg-rich magmas as a guide to their residual spinel peridotites; *J. Volcan. Geotherm. Res.* **59** 279–293.

Arai S 1994b Characterization of spinel peridotites by olivine–spinel compositional relationships: Review and interpretation; *Chem. Geol.* **113** 191–204, https://doi.org/10.1016/0009-2541(94)90066-3.

Arai S, Okamura H, Kadoshima K, Tanaka C, Suzuki K and Ishimaru S 2011 Chemical characteristics of chromian spinel in plutonic rocks: Implications for deep magma processes and discrimination of tectonic setting; *Isl. Arc* **20** 125–137; https://doi.org/10.1111/j.1440-1738.2010.00747.x.

Ballhaus C, Berry R F and Green D H 1990 Oxygen fugacity controls in the Earth's upper mantle; *Nature* **348**(**6300**) 437–440.

Ballhaus C, Berry R F and Green D H 1991 High-pressure experimental calibration of the olivine orthopyroxene-spinel oxygen barometer: Implications for the oxidation state for the upper mantle; *Contrib. Mineral. Petrol.* **107** 27–40.

Batanova V G, Suhr G and Sobolev A V 1998 Origin of geochemical heterogeneity in the mantle peridotites from the Bay of Islands ophiolite, Newfoundland, Canada: Ion probe study of clinopyroxenes; *Geochim. Cosmochim. Acta* **62(5)** 853–866.

Bédard É, Hébert R, Guilmette C, Lesage G, Wang C S and Dostal J 2009 Petrology and geochemistry of the Saga and Sangsang ophiolitic massifs, Yarlung Zangbo Suture Zone, Southern Tibet: Evidence for an arc–back-arc origin; *Lithos* **113**(**1**) 48–67.

Bodinier J L, Garrido C J, Chanefo I, Bruguier O and Gervilla F 2008 Origin of pyroxenite–peridotite veined mantle by refertilization reactions: Evidence from the Ronda peridotite (Southern Spain); *J. Petrol.* **49**(**5**) 999–1025.

Choi S H, Shervais J W and Mukasa S B 2008 Supra-subduction and abyssal mantle peridotites of the Coast Range ophiolite, California; *Contrib. Mineral. Petrol.* **156**(**5**) 551.

Coish R A and Gardner P 2004 Suprasubduction-zone peridotite in the northern USA Appalachians: Evidence from mineral composition; *Mineral. Mag.* **68**(**4**) 699–708.

Das S, Mukherjee B K, Basu A R and Sen K 2015 Peridotitic minerals of the Nidar ophiolite in the NW Himalaya: Sourced from the depth of the mantle transition zone and above; *Geol. Soc. Spec. Publ.* **412**(**1**) 271–286.

Das S, Basu A R and Mukherjee B K 2017 *In-situ* peridotitic diamond in Indus ophiolite sourced from hydrocarbon fluids in the mantle transition zone; *Geology* **45**(**8**) 755–758.

Dick H J B and Bullen T 1984 Chromian spinel as a petrogenetic indicator in abyssal and Alpine-type peridotites and spatially associated lavas; *Contrib. Mineral. Petrol.* **86**(**1**) 54–76.

Dijkstra A H, Barth M G, Drury M R, Mason P R and Vissers R L 2003 Diffuse porous melt flow and melt-rock reaction in the mantle lithosphere at a slow-spreading ridge: A structural petrology and LA-ICP-MS study of the Othris Peridotite Massif (Greece); *Geochem. Geophys. Geosyst.* **4**(**8**).

Dilek Y and Morishita T 2009 Melt migration and upper mantle evolution during incipient arc construction: Jurassic Eastern Mirdita ophiolite, Albania; *Isl. Arc* **18** 551–554.

Edwards S and Malpas J 1995 Multiple origins for mantle harzburgites: Examples from the Lewis Hills, Bay of Islands ophiolite, Newfoundland; *Can. J. Earth Sci.* **32**(**7**) 1046–1057.

Fabries J 1979 Spinel–olivine geothermometry in peridotites from ultramafic complex; *Contrib. Mineral. Petrol.* **6** 329–336.

Franz L and Wirth R 2000 Spinel inclusions in olivine of peridotite xenoliths from TUBAF seamount (Bismarck Archipelago/Papua New Guinea): Evidence for the thermal and tectonic evolution of the oceanic lithosphere; *Contrib. Miner. Petrol.* **140(3)** 283–295.

Godard M, Lagabrielle Y, Alard O and Harvey J 2008 Geochemistry of the highly depleted peridotites drilled at ODP Sites 1272 and 1274 (Fifteen–Twenty Fracture Zone, Mid-Atlantic Ridge): Implications for mantle dynamics beneath a slow spreading ridge; *Earth Planet. Sci. Lett.* **267** 410–425.

Gonzalez-Jimenez J M, Proenza J A, Gervilla F, Melgarejo J C, Blanco-Moreno J A, Ruiz-Sanchez R and Griffin W L 2011 High-Cr and high-Al chromitites from the Sagua de Tanamo district, Mayari-Cristal ophiolitic massif (eastern Cuba): Constraints on their origin from mineralogy and geochemistry of chromian spinel and platinum group elements; *Lithos* **125** 101–121.

Green D H, Falloon T J and Taylor W R 1987 Mantle-derived magmas-roles of variable source peridotite and variable CHO fluid compositions; In: *Magmatic Processes: Physicochemical Principles* (ed.) Mysen B O, *Geochem. Soc. Spec. Publ.* **1** 139–154.

Haggerty S E 1989 Upper mantle opaque mineral stratigraphy and the genesis of metasomites and alkali-rich melts; *Kimberlites and Related Rocks* **2** 687–699.

Hanghøj K, Kelemen P B, Hassler D and Godard M 2010 Composition and genesis of depleted mantle peridotites from the Wadi Tayin Massif, Oman Ophiolite; major and

trace element geochemistry, and Os isotope and PGE systematics; *J. Petrol.* **51**(**1–2**) 201–227.

Hébert R, Huot F, Wang C and Liu Z 2003 Yarlung Zangbo ophiolites (Southern Tibet) revisited: Geodynamic implications from the mineral record; *Geol. Soc. Spec. Publ.* **218**(**1**) 165–190.

Hellebrand E, Snow J E, Hoppe P and Hofmann A W 2002 Garnet field Melting and Late stage Refertilization in 'Residual' Abyssal Peridotites from the Central Indian Ridge; *J. Petrol.* **43**(**12**) 2305–2338.

Hellebrand E, Snow J E, Dick H J B and Hoffmann A W 2001 Coupled major and trace elements as indicators of extent of melting in mid-ocean-ridge peridotites; *Nature* **410** 677–681.

Himmelberg G R and Loney R A 1973 Petrology of the Vulcan Peak Alpine-type Peridotite, Southwestern Oregon; *Bull. Geol. Soc. Am.* **84**(**5**) 1585–1600.

Hirose K and Kawamoto T 1995 Hydrous partial melting of lherzolite at 1 GPa: The effect of H_2O on the genesis of basaltic magmas; *Earth Planet. Sci. Lett.* **133**(**3–4**) 463–473.

Ishii T, Robinson P T, Maekawa H and Fiske R 1992 Petrological studies of peridotites from diapiric serpentinite seamounts in the Izu–Mariana fore-arc, Leg 125; In: *Proceedings of the Ocean Drilling Program, Scientific Results* (eds) Fryer P, Pearce J A and Stokking L B, College Station, Texas, USA, **125** 445–485.

Jan M Q and Windley B F 1990 Chromian spinel-silicate chemistry in ultramafic rocks of the Jijal complex, Northwest Pakistan; *J. Petrol.* **31**(**3**) 667–715.

Johnson K T M, Dick H J B and Shimizu N 1990 Melting in the oceanic upper mantle: An ion microprobe study of diopsides in abyssal periodites; *J. Geophys. Res.* **95** 2661–2678.

Juteau T, Berger E and Cannat M 1990 Serpentinized, residual mantle peridotites from the MAR Median Valley, ODP hole 670A (21°10′N, 45°02′W, Leg 109): Primary mineralogy and geothermometry; In: *Proceedings of Ocean Drilling Program, Scientific Results*, **106/109**.

Kamenetsky V S, Crawford A J and Meffre S 2001 Factors controlling chemistry of magmatic spinel: An empirical study of associated olivine, Cr-spinel and melt inclusions from primitive rocks; *J. Petrol.* **42** 655–671, https://doi.org/10.1093/petrology/42.4.655.

Kapsiotis A 2014 Composition and alteration of Cr-spinels from Milia and Pefki serpentinized mantle peridotites, Pindos Ophiolite Complex, Greece; *Geol. Carpathica* **65** 83–95.

Kapsiotis A N 2016 Physiognomy and timing of metasomatism in the southern Vourinos ultramafic suite, NW Greece: A chronicle of consecutive episodes of melt extraction and stagnation in the Neotethyan lithospheric mantle; *Inter. J. Earth Sci.* **105**(**3**) 983–1013.

Kelemen P B 1990 Reaction between ultramafic rock and fractionating basaltic magma I. Phase relations, the origin of calc-alkaline magma series, and the formation of discordant dunite; *J. Petrol.* **31** 55–98.

Kelemen P B, Dick H J and Quick J E 1992 Formation of harzburgite by pervasive melt/rock reaction in the upper mantle; *Nature* **358**(**6388**) 635–641.

Khalil A E S and Azer M K 2008 Supra-subduction affinity in the Neoproterozoic serpentinites in the Eastern Desert, Egypt: Evidence from mineral composition; *J. Afr. Earth Sci.* **49** 136–152.

Le Fort P 1975 Himalayas: The collided range, Present knowledge of the continental arc; *Amer. J. Sci.* **275**(**1**) 1–44.

Liipo J, Vuollo J, Nykänen V, Piirainen T, Pekkarinen L and Tuokko I 1995 Chromites from the early Proterozoic Outokumpu–Jormua ophiolite belt: A comparison with chromites from Mesozoic ophiolites; *Lithos* **36**(**1**) 15–27.

Maheo G, Berttrand H, Guillot S, Villa I M, Keller F and Capiez P 2004 The South Ladakh Ophiolites (NW Himalaya, India): An intra-oceanic tholeiitic arc origin with implications for the closure of the Neo-Tethys; *Chem. Geol.* **203** 273–303.

Moghadam H S, Khedr M Z, Arai S, Stern R J, Ghorbani G, Tamura A and Ottley C J 2015 Arc-related harzburgite–dunite–chromitite complexes in the mantle section of the Sabzevar ophiolite, Iran: A model for formation of podiform chromitites; *Gondwana Res.* **27**(**2**) 575–593.

Molnar P and Tapponnier P 1975 Cenozoic tectonics of Asia: Effects of a continental collision; *Science* **189** 419–426.

Monnier C, Girardeau J, Maury R C and Cotten J 1995 Back-arc basin origin for the East Sulawesi ophiolite (eastern Indonesia); *Geology* **23**(**9**) 851–854.

Mukherjee B K, Sachan H K, Ogasawara Y, Muko A and Yoshioka N 2003 Carbonate-bearing UHPM rocks from the Tso-Morari region, Ladakh, India: Petrological implications; *Int. Geol. Rev.* **45**(**1**) 49–69.

Mysen B O and Kushiro I 1977 Compositional variations of coexisting phases with degree of melting of peridotite in the upper mantle; *Am. Mineral.* **62(9–10)** 843–865.

Nicolas A 1989 Structures of Ophiolites and Dynamics of Oceanic Lithosphere, Kluwer Academic, Dordrecht, 367p.

Nimis P and Taylor W R 2000 Single clinopyroxene thermobarometry for garnet peridotites, Part I. Calibration and testing of a Cr-in-Cpx barometer and an enstatite-in-Cpx thermometer; *Contrib. Mineral. Petrol.* **139**(**5**) 541–554.

Niu Y, Langmuir C H and Kinzler R J 1997 The origin of abyssal peridotites: A new perspective; *Earth Planet. Sci. Lett.* **152**(**1**) 251–265.

Ohara Y and Ishii T 1998 Peridotites from the southern Mariana forearc: Heterogeneous fluid supply in the mantle wedge; *Isl. Arc* **7** 541–558.

Okamura H, Arai S and Kim Y U 2006 Petrology of forearc peridotite from the Hahajima Seamount, the Izu-Bonin arc, with special reference to chemical characteristics of chromian spinel; *Mineral. Mag.* **70** 15–26.

Parkinson I J and Pearce J A 1998 Peridotites from the Izu-Bonin-Mariana forearc (ODP Leg 125): Evidence for mantle melting and melt–mantle interaction in a suprasubduction zone setting; *J. Petrol.* **39** 1577–1618.

Pearce J A, Barker P F, Edwards S J, Parkinson I J and Leat P T 2000 Geochemistry and tectonic significance of peridotites from the South Sandwich arc–basin system, South Atlantic; *Contrib. Mineral. Petrol.* **139**(**1**) 36–53.

Pearce J A, Alabaster T, Shelton A W and Searle M P 1981 The Oman ophiolite as a Cretaceous arc-basin complex: Evidence and implications; *Philos. Trans. R. Soc. London A* **300**(**1454**) 299–317.

Peighambari S, Ahmadipour H, Stosch H G and Daliran F 2011 Evidence for multi-stage mantle metasomatism at the Dehsheikh peridotite massif and chromite deposits of the Orzuieh coloured mélange belt, southeastern Iran; *Ore Geol. Rev.* **39** 245–264.

Pudsey C J 1986 The Northern Suture, Pakistan: Margin of a Cretaceous island arc; *Geol. Mag.* **123** 405–423.

Rampone E, Piccardo G B and Hofmann A W 2008 Multi-stage melt–rock interaction in the Mt. Maggiore (Corsica, France) ophiolitic peridotites: Microstructural and geochemical evidence; *Contrib. Mineral. Petrol.* **156**(**4**) 453–475.

Ravikant V, Pal T and Das D 2004 Chromites from the Nidar ophiolite and Karzok complex, Transhimalaya, Eastern Ladakh: Their magmatic evolution; *J. Asian Earth Sci.* **24** 177–184.

Sachan H K and Mukherjee B K 2003 Genesis of chromite in ophiolites from Indus Suture Zone, Ladakh, India: Evidence from mineral chemistry of solid inclusions in chromite; *Himal. Geol.* **24** 63–74.

Sachan H K, Mukherjee B K and Bodner R J 2007 Methane (CH_4) in upper mantle rocks from the Indus Suture Zone, Ladakh (India): Evidence from fluid inclusion and Raman spectroscopy; *Earth Planet. Sci. Lett.* **257** 47–59.

Sachan H K 2001 Supra-subduction origin of the Nidar ophiolitic sequence, Indus Suture Zone, Ladakh, India: Evidence from mineral chemistry of upper mantle rocks; *Ofioliti* **26**(**1**) 23–32.

Searle M P, Khan M A, Fraser J E and Gough S J 1999 The tectonic evolution of the Kohistan–Karakoram collision belt along the Karakoram Highway transect, north Pakistan; *Tectonics* **18** 929–949.

Sen K, Das S, Mukherjee B K and Sen K 2013 Bimodal stable isotope signatures of Zildat Ophiolitic Mélange, Indus Suture Zone, Himalaya: Implications for emplacement of an ophiolitic mélange in a convergent setup; *Int. J. Earth Sci.* **102(7)** 2033–2042.

Sharma K K and Gupta K R 1982 Northern Ladakh, a scene of explosive volcanic activity in early Cenozoic; *Contrib. Himal. Geol.* **2** 87–95.

Siddaiah N S 2001 Serpentinization, rodingitization, high-pressure metamorphism and mineralization in the Nidar ophiolite of Indus Suture Zone, Eastern Ladakh, Himalaya, India, Extended Abstract; In: *UHPM Workshop*, Waseda University, Japan, pp. 79–82.

Siddaiah N S and Masuda A 2001 Noble metals in the Nidar ophiolite of the Indus Suture zone, Eastern Ladakh, Himalaya, India*; Geol. Surv. India*, *Spec. Publ.* **58** 465–469.

Tahirkheli R K, Mattauer M, Proust F and Tapponnier P 1979 The India Eurasia suture zone in northern Pakistan: Synthesis and interpretation of recent data at plate scale, Geodynamics of Pakistan*, Geol. Surv. Pakistan*, *Quetta*, pp. 125–130.

Takazawa E, Frey F A, Shimizu N and Obata M 2000 Whole rock compositional variations in an upper mantle peridotite (Horoman, Hokkaido, Japan): Are they consistent with a partial melting process? *Geochim. Cosmochim. Acta* **64**(**4**) 695–716.

Taylor W R and Green D H 1988 Measurement of reduced peridotite-COH solidus and implications for redox melting of the mantle; *Nature* **332**(**6162**) 349.

Thakur V C and Bhat M I 1983 Interpretation of tectonic environment of Nidar ophiolite: A geochemical approach; *Geology of Indus Suture Zone of Ladakh*, pp. 21–31.

Thakur V C and Mishra D K 1984 Tectonic framework of Indus and Shyok Suture Zones in eastern Ladakh, Northwest Himalaya; *Tectonophys.* **101** 207–220.

Uysal I, Ersoy E Y, Karslı O, Dilek Y, Sadıklar M B, Ottley C J and Meisel T 2012 Coexistence of abyssal and ultra-depleted SSZ type mantle peridotites in a Neo-Tethyan Ophiolite in SW Turkey: Constraints from mineral composition, whole-rock geochemistry (major–trace–REE–PGE), and Re–Os isotope systematics; *Lithos* **132** 50–69.

Uysal I, Kaliwoda M, Karslı O, Tarkian M, Sadıklar M B and Ottley C J 2007 Compositional variations in whole rock and coexisting phases with partial melting and melt–peridotite interaction in an upper mantle section from the Ortaca Area, Southwestern Turkey; *Can. Mineral.* **45** 1471–1493.

Zhou M F, Sun M, Keays R R and Kerrich R W 1998 Controls on platinum-group elemental distributions of podiform chromitites: A case study of high-Cr and high-Al chromitites from Chinese orogenic belts; *Geochim. Cosmochim. Acta* **62** 677–688.

Zhou M F, Robinson P T, Malpas J, Edwards S J and Qi L 2005 REE and PGE geochemical constraints on the formation of dunites in the Luobusa ophiolite, Southern Tibet; *J. Petrol.* **46**(**3**) 615–639.

Corresponding editor: Rajneesh Bhutani